BJP British Journal of Pharmacology

DOI:10.1111/bph.12808
www.brjpharmacol.org

RESEARCH PAPER

Molecular basis of agonist docking in a human GPR103 homology model by site-directed mutagenesis and structure–activity relationship studies

C Neveu[1,2,3,*], F Dulin[3,4,*], B Lefranc[2,3], L Galas[2,3], C Calbrix[2,3], R Bureau[3,4], S Rault[3,4], J Chuquet[1,2,3], J A Boutin[5], L Guilhaudis[3,6], I Ségalas-Milazzo[3,6], D Vaudry[1,2,3], H Vaudry[1,2,3], J Sopkova-de Oliveira Santos[3,4] and J Leprince[1,2,3]

[1]*Inserm U982, Laboratory of Neuronal and Neuroendocrine Cell Differentiation and Communication, Neurotrophic Factors and Neuronal Differentiation Team, Institute for Research and Innovation in Biomedicine (IRIB),* [2]*Cell Imaging Platform of Normandy (PRIMACEN), IRIB, and* [6]*UMR 6014 CNRS, Analysis and Modeling Team, IRIB, University of Rouen, Mont-Saint-Aignan, France,* [3]*Normandie Univ, France,* [4]*UNICAEN, CERMN-FR CNRS INC3M-SF ICORE, University of Caen, Caen, France, and* [5]*Pôle d'Expertise Biotechnologie-Chimie-Biologie, Institut de Recherches Servier, Croissy-sur-Seine, France*

Correspondence
Jérôme Leprince, INSERM U982, Université de Rouen, Place Emile Blondel, Mont-Saint-Aignan 76821, France. E-mail: jerome.leprince@univ-rouen.fr

*Authors who equally contributed to this work.

Received
24 September 2013
Revised
4 April 2014
Accepted
15 May 2014

BACKGROUND AND PURPOSE

The neuropeptide 26RFa and its cognate receptor GPR103 are involved in the control of food intake and bone mineralization. Here, we have tested, experimentally, the predicted ligand-receptor interactions by site-directed mutagenesis of GPR103 and designed point-substituted 26RFa analogues.

EXPERIMENTAL APPROACH

Using the X-ray structure of the β_2-adrenoceptor, a 3-D molecular model of GPR103 has been built. The bioactive C-terminal octapeptide 26RFa$_{(19–26)}$, KGGFSFRF-NH_2, was docked in this GPR103 model and the ligand-receptor complex was submitted to energy minimization.

KEY RESULTS

In the most stable complex, the Phe-Arg-Phe-NH_2 part was oriented inside the receptor cavity, whereas the N-terminal Lys residue remained outside. A strong intermolecular interaction was predicted between the Arg^{25} residue of 26RFa and the Gln^{125} residue located in the third transmembrane helix of GPR103. To confirm this interaction experimentally, we tested the ability of 26RFa and Arg-modified 26RFa analogues to activate the wild-type and the Q125A mutant receptors transiently expressed in CHO cells. 26RFa (10^{-6} M) enhanced $[Ca^{2+}]_i$ in wild-type GPR103-transfected cells, but failed to increase $[Ca^{2+}]_i$ in Q125A mutant receptor-expressing cells. Moreover, asymmetric dimethylation of the side chain of arginine led to a 26RFa analogue, [ADMA^{25}]26RFa$_{(20–26)}$, that was unable to activate the wild-type GPR103, but antagonized 26RFa-evoked $[Ca^{2+}]_i$ increase.

CONCLUSION AND IMPLICATIONS

Altogether, these data provide strong evidence for a functional interaction between the Arg^{25} residue of 26RFa and the Gln^{125} residue of GPR103 upon ligand-receptor activation, which can be exploited for the rational design of potent GPR103 agonists and antagonists.

Abbreviations

$[Ca^{2+}]_i$, intracellular calcium concentration; ADMA, asymmetrical dimethyl arginine; DCM, dichloromethane; DIEA, N,N-diisopropylethylamine; ECL, extracellular loop; EH, extracellular helix; HBTU, O-benzotriazol-1-yl-N,N,N′,N′-tetramethyluronium hexafluorophosphate; HOBt, 1-hydroxy-benzotriazole; ICL, intracellular loop; IH, intracellular helix; NMP, N-methyl-2-pyrrolidone; PTX, *Pertussis* toxin; Q125A*h*GPR103, Gln125Ala human GPR103 mutant; SDMA, symmetrical dimethyl arginine; s*h*GPR103-CHO, stably transfected human GPR103 CHO; tA*h*GPR103-CHO, transiently transfected Q125A human GPR103 CHO; TBME, tertbutylmethylether; TFA, trifluoroacetic acid; t*h*GPR103-CHO, transiently transfected human GPR103 CHO; TIS, triisopropylsilane; TM, transmembrane; tpCHO, transiently pcDNA3.1-transfected CHO

Table of Links

TARGETS	LIGANDS
β2-adrenoceptor	
GPR103, QRFP receptor	Neuropeptide 26RFa, QRFP
Neuropeptide Y Y2 receptor	

This Table lists the protein targets and ligands in this article which are hyperlinked to corresponding entries in http://www.guidetopharmacology.org, the common portal for data from the IUPHAR/BPS Guide to PHARMACOLOGY (Pawson *et al.*, 2014) and the Concise Guide to PHARMACOLOGY 2013/14 (Alexander *et al.*, 2013).

Introduction

The neuropeptide 26RFa, which belongs to the RFamide superfamily, was originally isolated from the frog brain (Chartrel *et al.*, 2003) and subsequently cloned in rats and humans (Chartrel *et al.*, 2003; Fukusumi *et al.*, 2003). Analysis of the human 26RFa precursor indicates that pre-pro26RFa may generate several additional peptides including an N-terminally extended form, 43RFa (now known as QRFP) and a truncated form, $26RFa_{(20–26)}$ (GGFSFRF-NH_2,) that is strongly conserved across vertebrate species (Chartrel *et al.*, 2011; Leprince *et al.*, 2013). In the human hypothalamus and spinal cord, processing of the precursor generates both 26RFa and 43RFa (Bruzzone *et al.*, 2006), while in the rat and chicken brain, the mature form is 43RFa (Takayasu *et al.*, 2006) and 26RFa (Ukena *et al.*, 2010) respectively.

The search for a receptor target for 26RFa has led to the pairing with the former orphan receptor GPR103 (Fukusumi *et al.*, 2003; Jiang *et al.*, 2003). GPR103 is a class A (rhodopsin-like) 7-transmembrane (TM) domain GPCR that shares some sequence similarities with other RFamide receptors such as the neuropeptide FF-2 receptor, and with several neuropeptide receptors including the Y_2 neuropeptide Y receptor, the GAL_1 galanin receptor, the orexin and cholecystokinin receptors (Lee *et al.*, 2001; Jiang *et al.*, 2003). GPR103 activation with 26RFa or 43RFa induces an inhibition of cAMP formation (Fukusumi *et al.*, 2003), and an increase in intracellular calcium concentration ($[Ca^{2+}]_i$) in a *Pertussis* toxin (PTX)-independent manner, indicating that GPR103 is coupled to a $G_{i/0}$ and/or G_q protein (Fukusumi *et al.*, 2003). While only one *GPR103* gene is found in the human genome, two isoforms of the receptor have been cloned in rodents (Kampe *et al.*, 2006; Takayasu *et al.*, 2006). 26RFa binds mouse GPR103A and GPR103B with the same affinity (Takayasu *et al.*, 2006) and stimulates inositol trisphosphate via both rat receptors with similar efficacy (Kampe *et al.*, 2006).

In the CNS, 26RFa mRNA is expressed in discrete hypothalamic nuclei in rats (Chartrel *et al.*, 2003; Fukusumi *et al.*, 2003; Jiang *et al.*, 2003), mice (Takayasu *et al.*, 2006) and humans (Bruzzone *et al.*, 2006). 26RFa binding sites are widely distributed in the rat CNS (Bruzzone *et al.*, 2007) and GPR103 isoforms mRNAs are differentially expressed in the rat (Kampe *et al.*, 2006) and the mouse brain (Takayasu *et al.*, 2006). In humans, the highest concentrations of GPR103 are observed in the cerebral cortex, hypothalamus and vestibular nuclei (Jiang *et al.*, 2003). In human peripheral organs, the *GPR103* gene is expressed in the retina, pituitary, heart, kidney, testis and bone (Lee *et al.*, 2001; Fukusumi *et al.*, 2003; Baribault *et al.*, 2006).

GPR103-mediated 26RFa/43RFa effects include modulations of energy homeostasis, nociceptive transmission, locomotion, BP, heart rate, gonadotropin and aldosterone secretion, and bone mineralization (see Chartrel *et al.*, 2011; Leprince *et al.*, 2013). The wide spectrum of biological functions of 26RFa has made GPR103 a candidate target for therapeutic approaches concerning, for instance, feeding disorders and osteoporosis.

Elucidation of the structures of GPCRs and characterization of the mechanisms controlling ligand/receptor binding are required for rational drug design. An ideal method to address these issues would be the determination of the 3-D structure of the ligand/receptor complex by X-ray diffraction methods. However, the inherent characteristics of GPCRs, such as their hydrophobic nature, their flexibility and the requirement for membrane-like environments to insure proper folding, make crystal preparation particularly difficult.

Thus, computer-assisted molecular modelling is an alternative approach to acquire information on the architecture of GPCRs. Indeed, homology modelling methods allow to construct an atomic resolution model of the target protein from the solved 3-D structures of homologous proteins (Mobarec *et al.*, 2009; Simms *et al.*, 2009; Levit *et al.*, 2012).

In order to study GPR103–26RFa interactions, we have built a 3-D model of human GPR103 (*h*GPR103), based on the structure of the human β_2-adrenoceptor, that has subsequently been used to dock a biologically active human 26RFa (*h*26RFa) C-terminal fragment. A candidate residue in the binding pocket has been identified as interacting with a 26RFa amino acid. We have experimentally validated the *h*GPR103/*h*26RFa model using receptor site-directed mutagenesis and synthetic *h*26RFa analogues, and characterized this interaction as a GPR103 activation switch.

Methods

Molecular modelling

Receptor model. First, the sequence of *h*GPR103 was retrieved from the UniProt Knowledgebase (UniProtKB) (Jain *et al.*, 2009) (accession number: Q96P65). Taking into account the relatively high sequence homology of *h*GPR103 with the β_2-adrenoceptor, as well as the high resolution (2.4 Å) of the β_2-adrenoceptor-T4 lysozyme chimera bound to the partial inverse agonist carazolol (accession number: 2RH1), we have built a first *h*GPR103 model on this template. *h*GPR103 and human β_2-adrenoceptor sequences have been aligned using different algorithms in the @tome server (Labesse and Mornon, 1998). Then, the alignment between the two sequences has been manually optimized and evaluated with the TITO program (Labesse and Mornon, 1998). The disulfide bond (C^{118}–C^{201}) between the TM3 domain and extracellular loop (ECL) 2 of *h*GPR103 was conserved. This alignment was used as the basis for the homology modelling with the Modeller software (Eswar *et al.*, 2008), an automatic comparative modelling program. The folding quality of the model was considered to be good according to the 3-D evaluation tools, that is Verify3D (Eisenberg *et al.*, 1997) and Eval23D (Gracy *et al.*, 1993). Sequence alignment figure was made with the ESPript software (Gouet *et al.*, 2003).

Docking studies. Docking of $26RFa_{(19–26)}$ into *h*GPR103 was carried out using the NMR structure of the C-terminal part ($26RFa_{(19–26)}$) of *h*26RFa in methanol (Thuau *et al.*, 2005) by means of the GOLD program with the default parameters (Jones *et al.*, 1995; 1997). This program applies a genetic algorithm to explore conformational spaces and ligand-binding modes. To evaluate the proposed ligand poses, the GoldScore fitness function was applied. The binding site in the *h*GPR103 model was defined as a 15 Å sphere centred on a point (–33.671, 6.986, 8.164) located in the centre of the cavity. During this docking procedure, we paid special attention to some amino acids in the binding site, which were kept flexible such as the Gln^{125} residue.

Model refinement (energy minimization). The selected *h*GPR103/$26RFa_{(19–26)}$ complexes were optimized using the CHARMM software (Brooks *et al.*, 1983) with parameter set-22 (MacKerell *et al.*, 1988). The van der Waals interactions were truncated using a switching function, and the electrostatic ones using a force switching function (between 8 and 13 Å). The vacuum dielectric constant was used during all calculations. The SHAKE constraint was used for the hydrogen atoms. As we would optimize only the side chain orientations, the complexes were solvated by TIP3P (Jorgensen *et al.*, 1983) water molecules (water molecules clashing with the protein were removed), and surrounded by identical translated images of itself using periodic boundary conditions. To allow only the side chains optimization, the backbone atoms of TM helices were constrained. The two complex models were first minimized to an RMS energy gradient $<10^{-4}$ kcal mol^{-1}/Å and after a quick dynamic simulation using Verlet algorithm was performed. The system was heated to 300 K at 6 ps and then temperature-equilibrated during 50 ps.

Site-directed mutagenesis

Mutant receptor construct. The entire coding region of *h*GPR103, containing the Flag M2 epitope sequence (DYKDDDDK) at its 3′-end, was subcloned into the pcDNA3.1(+) mammalian expression vector (Invitrogen, Life Technologies, Saint-Aubin, France) as previously described (Le Marec *et al.*, 2011). The pcDNA3.1(+)/*h*GPR103_M2 plasmid, inserted into a TOP-10 dam^+ *Escherichia coli* strain for methylation of parental DNA, was isolated by a rapid plasmid extraction procedure using the QIAprep Spin Miniprep kit (Qiagen, Courtabœuf, France). Standard-purified mutagenesis primers were designed following the QuickChange Site-directed Mutagenesis kit guidelines (Stratagene, Agilent Technologies, Massy, France). The sequences of the primers were (mutagenic positions underlined): forward 5′-AAGATGGTGCCA TTTGTCGCGTCTACCGCTGTTGTGAC-3′, reverse 5′-GTCAC AACAGCGGTAGACGCGACAAATGGCACCATCTT-3′. Mutations were introduced into the *h*GPR103 sequence using the QuickChange II Site-directed Mutagenesis kit (Stratagene, Agilent Technologies) according to the manufacturer's protocol. The mutagenesis reactions were carried out in 50 µL total volume using 50 ng of plasmid DNA, 2.5 U of PfuTurbo DNA polymerase and 125 ng of each primer. The cycling conditions were a 30 s initial denaturation at 95°C, 18 cycles with 30 s denaturation at 95°C, 1 min annealing at 55°C and 6.5 min extension at 68°C. The product was restricted with 10 U of DnpI and incubated for 1 h at 37°C to digest selectively the parental, methylated strands. Then, 1 µL of the reaction medium was used for transformation of XL1-Blue cells by thermal shock and cells were plated for selection of ampicillin resistant clones. Single transformant clones were grown overnight at 37°C in 5 mL LB-Broth completed with 80 µg mL^{-1} ampicillin. A rapid plasmid extraction was carried out from a 4 mL culture using the QIAprep Spin Miniprep kit (Qiagen).

Sequencing. Sequencing was carried out following the GenomeLab Dye Terminator cycle Sequencing Quick Start kit (Beckman Coulter, Villepinte, France) to assess whether the mutation had been incorporated. Forward primers were: 5′-TAATACGACTCACTATAGGG-3′; 5′-CCTGCATTGCTGTG GAAAGGCAC-3′; and reverse primers were: 5′-GCCTCGAC

TGTGCCTTCTA-3′; 5′-TGCCTTTGTGCTGGAGAGAAGGT-3′. The PCR reaction was performed in a 20 µL total volume using 450 ng (100 fmol) of dsDNA, 1.6 µM of primers and all other reagents of the kit. The cycling conditions were 30 cycles with 20 s at 96°C, 20 s at 50°C and 4 min at 60°C. The PCR product was precipitated with ethanol and templates were loaded into a capillary sequencer SEQ8000 (Beckman Coulter).

Cell culture and transfection. Non-transfected host CHO cells and stably transfected human GPR103 CHO (s*h*GPR103-CHO) cells were obtained as previously described (Rodriguez *et al*., 2001; Le Marec *et al*., 2011). The cells were maintained in Ham-F12 medium supplemented with 10% (v/v) FBS (inactivated at 56°C for 30 min), 2 mM glutamine, 500 IU mL^{-1} penicillin and 100 µg mL^{-1} streptomycin. Expression of $G\alpha_{16}$ was maintained using selection antibiotic hygromycin B (200 µg mL^{-1}) and that of *h*GPR103 using geneticin G418 (500 µg mL^{-1}) (Gibco, Life Technologies). Native pcDNA3.1(+)/*h*GPR103_M2, mutant pcDNA3.1(+)/Gln^{125}Ala-*h*GPR103_M2 and empty pcDNA3.1(+) plasmids were transfected into CHO-$G\alpha_{16}$ cells by nucleofection using the Amaxa cell line nucleofector T kit as described by the manufacturer (Lonza, Levallois-Perret, France). CHO cells were used at 80% confluency. One million cells per sample were resuspended at room temperature in 100 µL nucleofector solution, combined with 2 µg plasmid DNA. Cells were electroporated with use of the nucleofection programme U-023. Transfected cells were transferred into the culture plate containing culture medium.

RT-PCR. Expression of *h*GPR103 or Gln125Ala human GPR103 mutant (Q125A*h*GPR103) was verified by RT-PCR. Cells (5×10^5) were lysed and total RNA was extracted using the TRI Reagent kit (Sigma-Aldrich, Saint-Quentin Fallavier, France) (Chomczynski and Sacchi, 1987). mRNA (1.25 µg) was reverse-transcribed using the ImProm-II kit (Promega, Charbonnières-les-Bains, France). PCR reactions were performed in a volume of 25 µL containing 5 µL buffer, 0.5 µL dNTP, 1 µL forward and reverse primers, 5 µL cDNA and 0.5 µL GoTaq DNA polymerase. Primer sequences used for *h*GPR103 and Q125A*h*GPR103 amplification were: forward 5′-TTAACATTACCCCGGAGCAG-3′ and reverse 5′-TAATCG GTACCATGCCCACT-3′. The cycling conditions were: 1 cycle at 94°C during 5 min, followed by 35 cycles of 30 s at 94°C, 30 s at 52°C and 1.5 min at 72°C, and terminated by 1 cycle at 72°C during 5 min. The amplified cDNAs were then analysed after gel migration (agarose 1%, Tris-acetate-EDTA 0.5X, 2 µg/100 mL de BET- 100 V during 20 min).

Immunocytochemistry. Non-transfected host CHO, s*h*GPR103-CHO, transiently transfected human GPR103 CHO (t*h*GPR103-CHO) and tA*h*GPR103-CHO cells were incubated for 3 days into 24-well culture plates containing cover glasses (15 mm diameter), previously coated with poly-L-lysine (10 ng mL^{-1}), at a density of 100 000 transiently transfected cells per well or of 30 000 stably transfected cells per well. Cells were incubated with medium alone or with cycloheximide (3×10^{-4} M) (Sigma-Aldrich) during 90 min and *h*26RFa (10^{-6} M) during 2 min, and fixed with 2% paraformaldehyde for 10 min. After rinsing in PBS, cells were permeabilized by 0.1% saponin during 20 min and incubated for 1 h with PBS containing 0.1% saponin, 1% BSA, 1/50 (v/v) normal goat serum, before adding a mouse anti-Flag M2 antibody (1/300) (Sigma-Aldrich) during 40 min. Cells were rinsed and incubated with an Alexafluor 488-conjugated goat anti-mouse IgG antibody (1/250) (Molecular Probes, Life Technologies) during 30 min. Nuclei were stained with DAPI. The cover glasses were fixed on the slides by Mowiol (Sigma-Aldrich) and the fluorescence was examined using an inverted confocal microscope (Leica TCS SP5, Nanterre, France).

Calcium mobilization assays. Changes in intracellular Ca^{2+} concentrations induced by *h*26RFa in non-transfected host CHO, transiently pcDNA3.1-transfected CHO (tpCHO), s*h*GPR103-CHO, t*h*GPR103-CHO and tA*h*GPR103-CHO cells were measured on a benchtop scanning fluorometer Flexstation III (Molecular Devices, Sunnyvale, CA, USA) as previously described (Le Marec *et al*., 2011). Briefly, 96-well assay black plates with clear bottom (Corning International, Avon, France) were seeded at a density of 100 000 transiently transfected cells per well 36 h prior to assay or 20 000 stably transfected cells per well 48 h prior to assay. Cells were loaded with 2 µM fluo-4AM (Invitrogen) during 1 h, rinsed three times and incubated 30 min with standard HBSS containing 2.5 mM probenecid and 5 mM HEPES. HBSS, *h*26RFa (at final concentrations ranging from 10^{-8} to 10^{-6} M) and ATP (10^{-4} M) were successively added 17, 60 and 180 s after the onset of acquisition and the fluorescence intensity was recorded over a 5 min period. A xenon lamp was used as an excitation source. The wavelengths of excitation (485 nm) and emission (525 nm) of fluo-4AM were selected by two monochromators included in the device equipped with a bottom reading probe.

Peptide synthesis

Reagents. All Fmoc-amino acid residues, O-benzotriazol-1-yl-N,N,N′,N′-tetramethyluronium hexafluorophosphate (HBTU) and 1-hydroxy-benzotriazole (HOBt) were purchased from PolyPeptide (Strasbourg, France) or Christof Senn Laboratories (Dielsdorf, Switzerland). The Rink amide 4-methylbenzhydrylamine resin was from VWR International (Fontenay-sous-Bois, France). N,N-diisopropylethylamine (DIEA), piperidine, trifluoroacetic acid (TFA) and triisopropylsilane (TIS) were supplied by Acros Organics (Geel, Belgium). N-methyl-2-pyrrolidone (NMP), dichloromethane (DCM) and other reagents were from Sigma-Aldrich. Acetonitrile was from Fisher Scientific (Illkirch, France).

Synthesis. *h*26RFa, $26RFa_{(19–26)}$ and $26RFa_{(20–26)}$ analogues were synthesized (0.1 mmol scale) by the solid phase methodology on a Rink amide 4-methylbenzhydrylamine resin using a 433A Applied Biosystems peptide synthesizer (Applera-France, Courtaboeuf, France) and the standard Fmoc manufacturer's procedure as previously described (Le Marec *et al*., 2011). All Fmoc-amino acids (1 mmol, 10 eq.) were coupled by *in situ* activation with HBTU/HOBt (1.25 mmol : 1.25 mmol, 12.5 eq.) and DIEA (2.5 mmol, 25 eq.) in NMP. Peptides were deprotected and cleaved from the resin by adding 10 mL of the mixture TFA/TIS/H_2O (99.5:0.25:0.25, v/v/v) for 120 min at room temperature.

After filtration, crude peptides were precipitated by addition of tertbutylmethylether (TBME), centrifuged (4500 rpm), washed twice with TBME, and freeze-dried. The synthetic peptides were purified by reversed-phase HPLC on a 2.2 × 25 cm Vydac 218TP1022 C_{18} column (Grace, Epernon, France) using a linear gradient (10–50% over 45 min) of CH_3CN/TFA (99.9:0.1; v/v) at a flow rate of 10 mL min^{-1}. Analytical HPLC, performed on a 0.46 × 25 cm Vydac 218TP54 C_{18} column (Grace), showed that the purity of all peptides was >99.9% (Table 2). The purified peptides were characterized by MALDI-TOF mass spectrometry on a Voyager DE PRO (Applera-France) in the reflector mode with α-cyano-4-hydroxycinnamic acid as a matrix.

Results

*h*GPR103 *model*

Among the solved GPCR structures that were available in the PDB database when we started this study, *h*GPR103 exhibited 20, 23, 22, 23, 26, 24, 23 and 22% sequence identity with bovine and squid rhodopsins, bovine opsin, avian (turkey) β_1- and human β_2-adrenoceptors, human A_{2A} adenosine receptor, human CXCR4 and human dopamine D_3 receptor respectively. Manual adjustments of important structural and functional features of class A GPCRs have been incorporated to the initial alignment such as the conserved disulfide bridge between the N-terminal extremity of the TM3 domain (Cys^{118}) and the ECL2 (Cys^{201}). Sequence alignment showed substantial homology within TM helices ranging from 45 to 75% for TM4 and TM7, respectively (Figure 1). Loops connecting the TM helices were modelled on the basis of the template loops except for intracellular loop (ICL) 3, which was replaced by lysozyme T4 in the β_2-adrenoceptor to facilitate its crystallization. The modelled structure of *h*GPR103 remained very close to the X-ray structure of human β_2-adrenoceptors. Indeed, root mean square deviation on Cα TM residues was 0.495 Å. All residues of the *h*GPR103 model were in favoured regions of the Ramachandran plot. Like the structure of the β_2-adrenoceptor, the *h*GPR103 model exhibited two short non-TM helices, in ECL2 (extracellular helix, EH; Ile^{188} to Lys^{196}; Figure 1) and in the intracellular C-terminal tail (intracellular helix, IH; Glu^{337} to Val^{347}; Figure 1), IH being present in all rhodopsin-like GPCRs (Katragadda *et al.*, 2004). The *h*GPR103 model encompassed a relatively narrow and deep binding pocket on the extracellular face of the protein for harbouring endogenous or synthetic ligands.

Molecular docking of $26RFa_{(19–26)}$ *into the h*GPR103 *model*

The C-terminal octapeptide $26RFa_{(19–26)}$ was docked in the *h*GPR103 model. Among the proposed docking poses, only

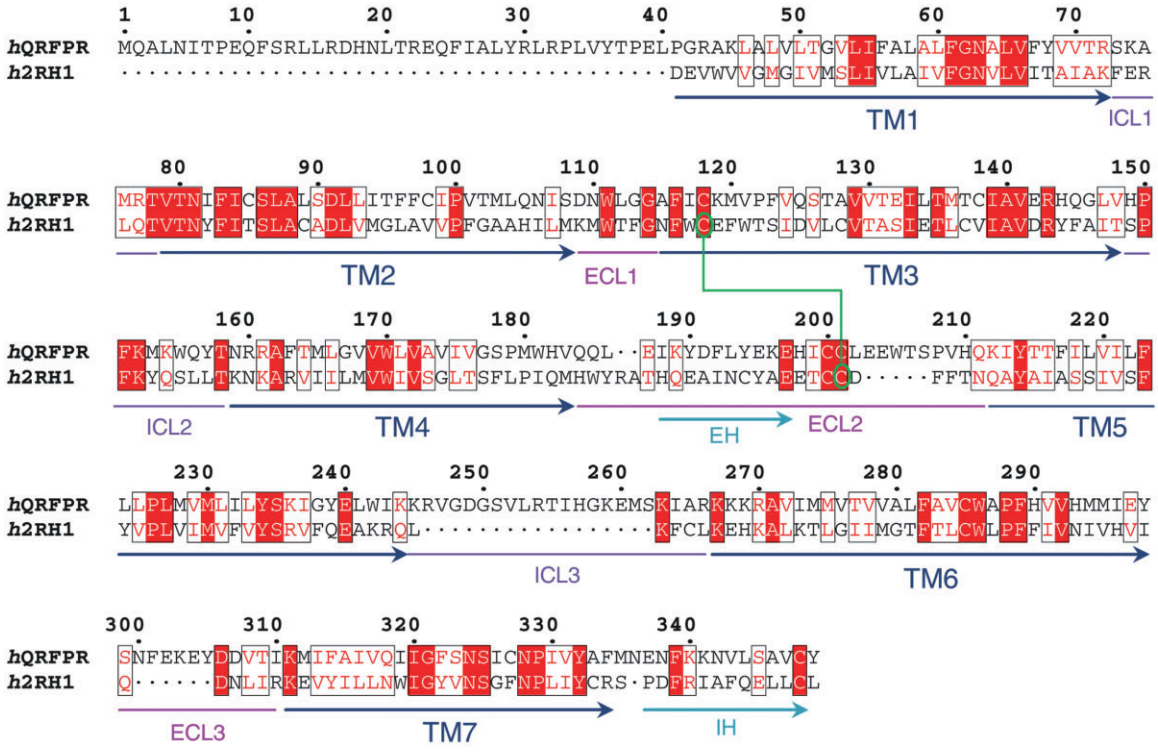

Figure 1

Amino acid sequence alignment of *h*GPR103 (*h*QRFPR) and human β_2-adrenoceptor (*h*2RH1). TM (TM1–7) helices are delimited by horizontal dark blue arrows. ICLs (1–3) and ECLs (1–3) are indicated by horizontal purple and pink lines respectively. The EH in ECL2 and the IH in the C-terminal tail are delimited by horizontal light blue arrows. The disulfide bridge between the Cys^{118} and Cys^{201} residues of *h*GPR103 is also indicated. Fully conserved amino acids are highlighted with red boxes and highly conserved amino acids with white boxes.

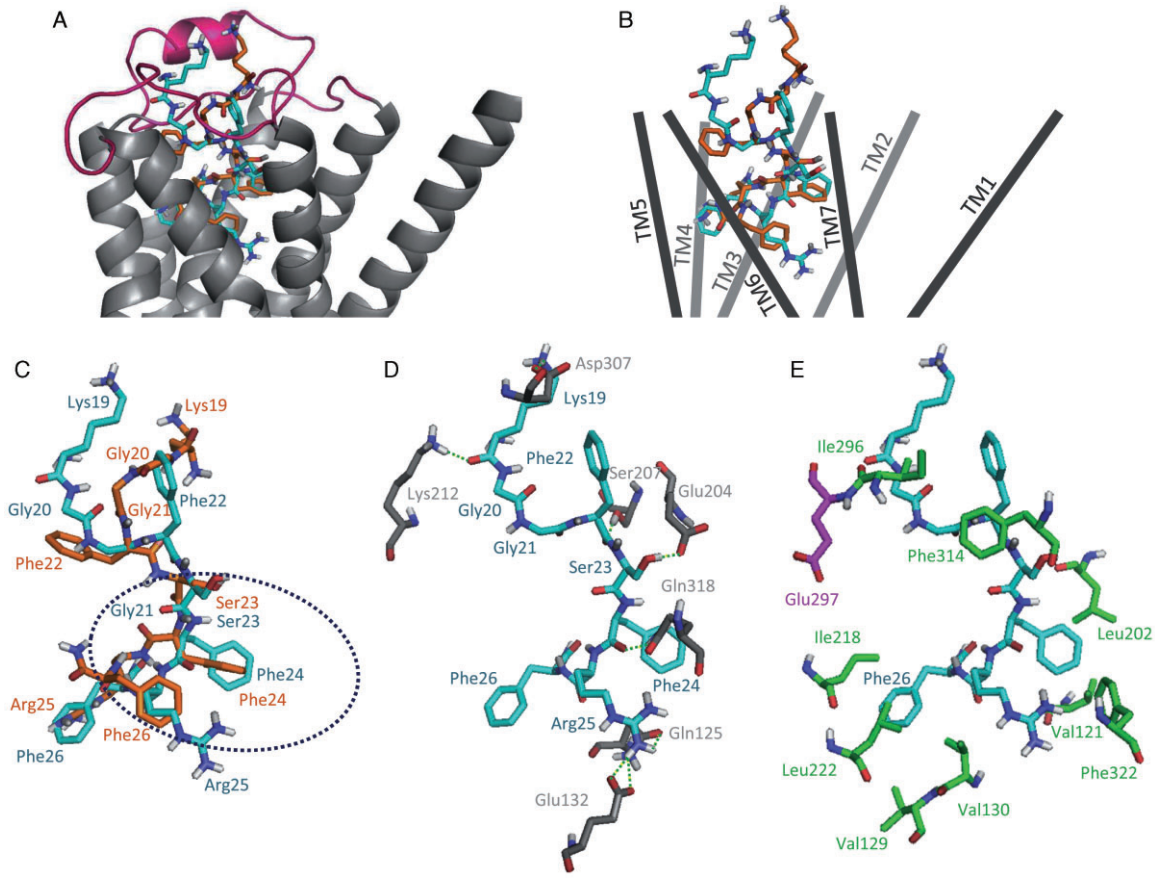

Figure 2

26RFa$_{(19–26)}$ heptapeptide docked in the *h*GPR103 receptor model. The 26RFa$_{(19–26)}$ backbone and side chains are highlighted by sticks (solution one is coloured in orange and solution two in cyan), ECLs 1, 2 and 3 are represented by pink ribbons and TM domains by dark grey ribbons (A) or schematic bars (B). (C) Focus of the superimposition of the two solutions. The amino acids of 26RFa$_{(19–26)}$ are labelled. The middle part of the hexapeptides where amino acids of the two solutions are almost superimposed is dash-circled in dark blue (Ser^{23} and Phe^{24}). (D,E) Detailed views of the interactions between 26RFa$_{(19–26)}$ in the position observed in solution two. Amino acids of *h*GPR103, which established H-bonds (green dash-line) with 26RFa$_{(19–26)}$ are highlighted by grey sticks (D) and hydrophobic amino acids are represented in green. The Glu^{297} residue of *h*GPR103 is displayed by pink sticks. The orientation of the complex is maintained in views A–C and slightly shifted for better viewing in panels D and E. Figures were drawn with PYMOL, version 1.1eval (DeLano Scientific, 2002, San Carlo, CA, USA).

two appeared to be realistic, corresponding to the highest score fits from GoldScore fitness function. In both poses, the C-terminal Phe-Arg-Phe-NH_2 part was oriented inside the binding cavity whereas the N-terminal Lys^{19} residue of the octapeptide remained outside (Figure 2A and B). The two *h*GPR103/26RFa$_{(19–26)}$ complexes were energy minimized, keeping the TM helix backbones fixed, to optimize the orientation of all side chains within the cavity. A complete description of the intermolecular interactions between 26RFa$_{(19–26)}$ and *h*GPR103 is listed in Table 1. In the two poses, 26RFa$_{(19–26)}$ interacted with all TM domains except the TM1 and TM2 helices (Figure 2A and B). The major differences between these two solutions occurred in the position of the N-terminal and C-terminal regions. Indeed, in the central region of 26RFa$_{(19–26)}$, Ser^{23} and Phe^{24} were rather well superimposed in both solutions (Figure 2C). In the N-terminal part, the Phe^{22} residue of each solution was superimposed with the Gly^{21} residue of the other solution, steering Lys^{19} and Gly^{20} in opposite directions. In the C-terminal part, the Arg^{25} and Phe^{26} residues were also oriented poles apart with a superimposition of Arg^{25} of one solution with the Phe^{26} of the other (Figure 2C). Among the two complexes, we have selected the second one, as it presented the highest interaction energy between the two partners ($|\Delta E|$ ~ 340.2 kcal mol^{-1} compared with $|\Delta E|$ ~ 210.8 kcal mol^{-1} for the first solution, Table 1). In this selected solution, the strongest interactions, according to interaction energy per residue, were established between the guanidine function of the Arg^{25} residue of the peptide and the amide side chain of the Gln^{125} moiety situated on the top of the TM3 helix ($|\Delta E|$ ~ 101.5 kcal mol^{-1}), and between the ε-amine group of the Lys^{19} residue and the side chain of the Asp^{307} residue of ECL3 ($|\Delta E|$ ~ 120.4 kcal mol^{-1}) (Table 1; Figure 2D). Furthermore, in this solution, the Phe^{26} residue of 26RFa$_{(19–26)}$ interacted with a hydrophobic region of the binding pocket (Ile^{218}, Leu^{222}, Val^{129} and Val^{130}) strengthening the stability of the complex (Table 1; Figure 2E). Indeed, the

Table 1

List of 26RFa$_{(19–26)}$ and *h*GPR103 residues in close contact and associated energy

	***h*GPR103**[a,b]		**|ΔE| (kcal mol^{-1})**	
26RFa$_{(19–26)}$	**Pose 1**	**Pose 2**	**Pose 1**	**Pose 2**
Lys^{19} bb	*Ser^{207}* sc	*Lys^{212}* sc	21.7	120.4
Lys^{19} sc		*Asp^{307}* sc		
Gly^{20}			5.9	7.1
Gly^{21}			6.4	9.1
Phe^{22} bb	*Ser^{207}* sc		26.1	28.2
Phe^{22} sc	**Ile^{296}** sc	**Ile^{296}** sc, **Phe^{314}** sc		
Ser^{23} sc	*Glu^{204}* sc, *Gln^{318}* sc	*Glu^{204}* sc	29.8	34.5
Phe^{24} bb	*Gln^{318}* sc		18.5	14.5
Phe^{24} sc	**Leu^{202}** sc, **Val^{121}** sc, **Phe^{322}** sc, **Pro^{122}** sc			
Arg^{25} bb	*Gln^{125}* sc		70.9	101.5
Arg^{25} sc	*Val^{176}* bb, *Gly^{177}* bb, *Ser^{126}* sc	*Gln^{125}* sc, *Glu^{132}* sc		
Phe^{26} bb	*His^{290}* sc		31.5[c]	24.9[d]
Phe^{26} sc	**Phe^{289}** sc, **Phe^{322}** sc, **Val^{129}** sc, **Trp^{286}** sc	**Ile^{218}** sc, **Leu^{222}** sc, **Val^{129}** sc, **Val^{130}** sc		
			210.8	340.2

[a]Residues with H-bond interacting atom are indicated in italic. [b]Residues with hydrophobic/aromatic interacting atoms are indicated in bold. [c]Hydrophobic contribution counts for 18.8 kcal mol^{-1}. [d]Hydrophobic contribution counts for 20.5 kcal mol^{-1}. bb, backbone; sc, side chain (sc).

hydrophobic contribution in the interaction energy at this point was 18.8 and 20.5 kcal mol^{-1} in poses 1 and 2, respectively (Table 1).

*Expression of the h*GPR103 *mutant*

The proposed molecular model 2 (Figure 2D and E) was challenged by probing the molecular partner of the Arg^{25} residue of 26RFa$_{(19–26)}$. The Q125A*h*GPR103 has been engineered and tested for its activation by *h*26RFa. Expression of *h*GPR103 and its mutant in transiently transfected cells was verified by RT-PCR (Figure 3). s*h*GPR103-CHO, t*h*GPR103-CHO and transiently transfected Q125A-GPR103 CHO cells (tA*h*GPR103-CHO) were positive for a wild-type or mutant *h*GPR103 expression, whereas non-transfected host CHO and tpCHO cells exhibited neither wild-type nor mutant *h*GPR103 transcripts (Figure 3). Expression and targeting at the cell surface of *h*GPR103 or Q125A*h*GPR103 proteins have been verified by immunofluorescence microscopy using antibodies against the Flag M2 epitope, which was incorporated at the C-terminal extremity of wild-type and mutant receptors (Figure 4). Confocal microscope analysis of s*h*GPR103-CHO, t*h*GPR103-CHO and tA*h*GPR103-CHO cells in resting conditions showed that all three receptors were primarily localized in the cytoplasm in the absence (Figure 4 A_1, A_2 and A_3) as in the presence of cycloheximide (Supporting Information Figure S1). After treatment with cycloheximide and *h*26RFa, as previously described (Iturrioz *et al.*, 2010), only the cell lines stably and transiently transfected with the wild-type receptor, that is s*h*GPR103-CHO and t*h*GPR103-CHO cells, respectively, displayed intense

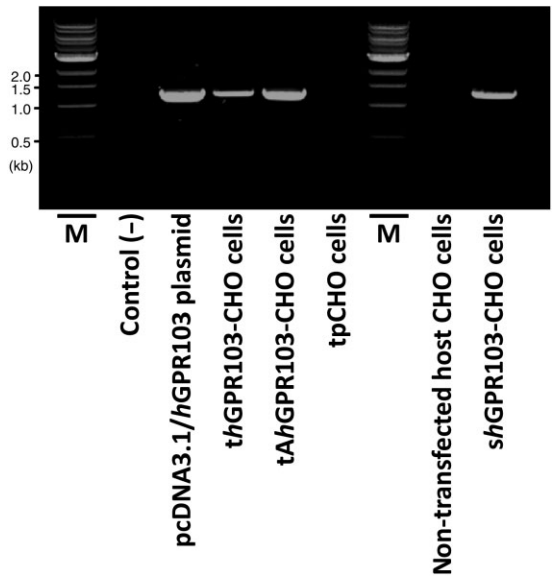

Figure 3

Expression analysis of *h*GPR103 and Q125A*h*GPR103 mRNA. RT-PCR was performed on pcDNA3.1/*h*GPR103 plasmid, t*h*GPR103-CHO cells, tA*h*GPR103-CHO cells, tpCHO cells, non-transfected host CHO cells and s*h*GPR103-CHO cells. Total RNAs were retrotranscribed and used for PCR amplification of *h*GPR103 and Q125A*h*GPR103 cDNA fragments with the same specific primer. As expected, the amplified products, analysed on 1% agarose gel corresponded to 1294 bp. PCR amplification products of s*h*GPR103-CHO and pcDNA3.1/*h*GPR103 plasmid were used as positive controls. M, markers.

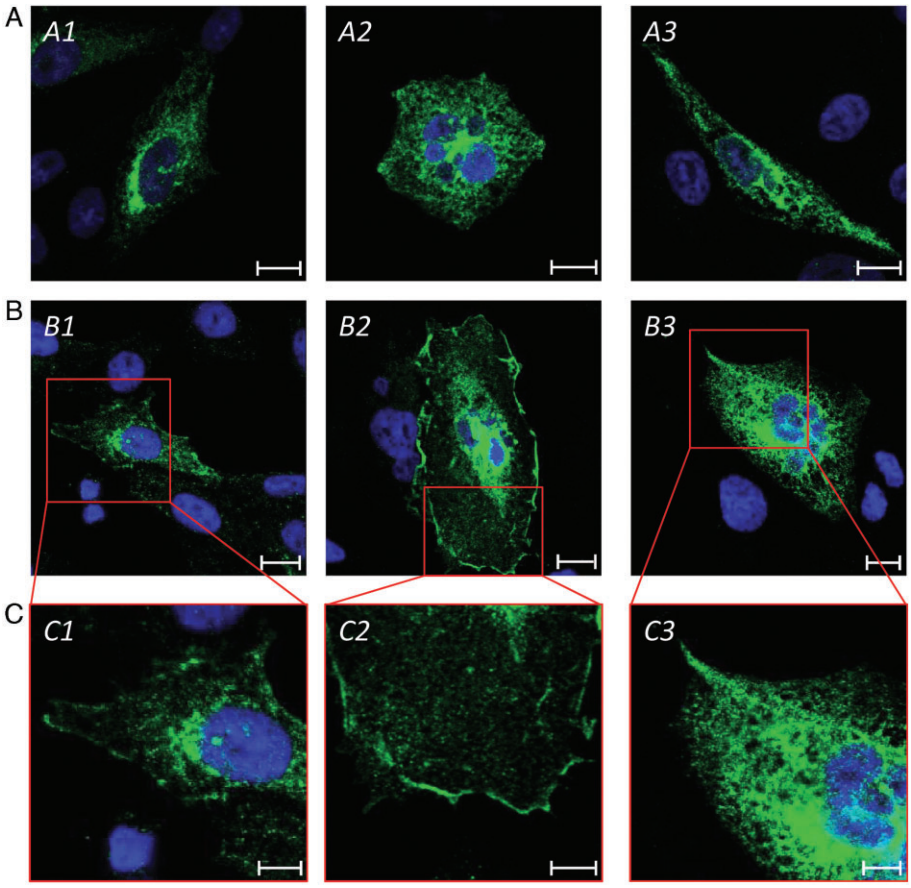

Figure 4

Confocal images showing localization of the Flag M2-tagged *h*GPR103 and Q125A*h*GPR103 in stably and transiently transfected CHO cells in the absence or presence of cycloheximide and *h*26RFa. Immunocytochemistry was performed with a primary antibody against the Flag M2 and a secondary antibody labelled with green-fluorescence Alexafluor 488. Nuclei were stained with DAPI (blue). (A) In the absence of cycloheximide and *h*26RFa, the Flag M2-tagged receptors were detected in s*h*GPR103-CHO cells (A1), in t*h*GPR103-CHO cells (A2) and in tA*h*GPR103-CHO cells (A3). Scale bars = 10 μm. (B) s*h*GPR103-CHO cells (B1), t*h*GPR103-CHO cells (B2) or tA*h*GPR103-CHO cells (B3) were incubated with cycloheximide (3×10^{-4} M) for 90 min and *h*26RFa (10^{-6} M) for 2 min. Scale bars = 10 μm. (C) Higher magnification showing the occurrence of the wild-type receptor (C1 and C2) and the absence of the mutant receptor (C3) at the cell surface. Scale bars = 5 μm.

immunofluorescence staining at the plasma membrane (Figure 4B_1, B_2, C_1 and C_2). In contrast, in tA*h*GPR103-CHO cells, the fluorescence remained localized in the cytoplasm (Figure 4B_3 and C_3). Finally, non-transfected host CHO cells were not stained, and non-permeabilized s*h*GPR103-CHO cells did not exhibit any immunofluorescence (data not shown).

*Effect of h*26RFa *on mutant h*GPR103

In order to confirm the importance of the Gln^{125} residue, located inside the binding cavity, in *h*GPR103 recognition and/or activation processes, the ability of *h*26RFa to activate the mutant receptor Q125A*h*GPR103 was determined by assessing the Ca^{2+} response of transfected cells (Figure 5). As a negative control, it was verified that administration of culture medium alone did not cause an increase in $[Ca^{2+}]_i$ in any of the cell types studied that is host CHO, tpCHO, s*h*GPR103-CHO, t*h*GPR103-CHO and tA*h*GPR103-CHO cells (Figure 5, arrow 1). As a positive control, ATP (10^{-4} M) was shown to induce a 200–300% $[Ca^{2+}]_i$ rise in all cell types (Figure 5, arrow 3). *h*26RFa (10^{-6} M) had no effect on calcium mobilization in non-transfected host CHO and tpCHO cells (Figure 5A, arrow 2), whereas it enhanced $[Ca^{2+}]_i$ by 200 and 150% in s*h*GPR103-CHO and t*h*GPR103-CHO cells, respectively (Figure 5B and C, arrow 2). In contrast, *h*26RFa (10^{-6} M) failed to increase $[Ca^{2+}]_i$ in tA*h*GPR103-CHO cells (Figure 5D, arrow 2).

*Effect of Arg-modified h*26RFa *analogues on wild-type h*GPR103

To further investigate the contribution of the side chain of the Arg moiety of *h*26RFa in the activation process of *h*GPR103, we have synthesized five analogues of the C-terminal heptapeptide substituted at position 25 and tested their effect on $[Ca^{2+}]_i$ in s*h*GPR103-CHO cells (Table 2). Replacement of the Arg^{25} residue by a lysine, an ornithine or

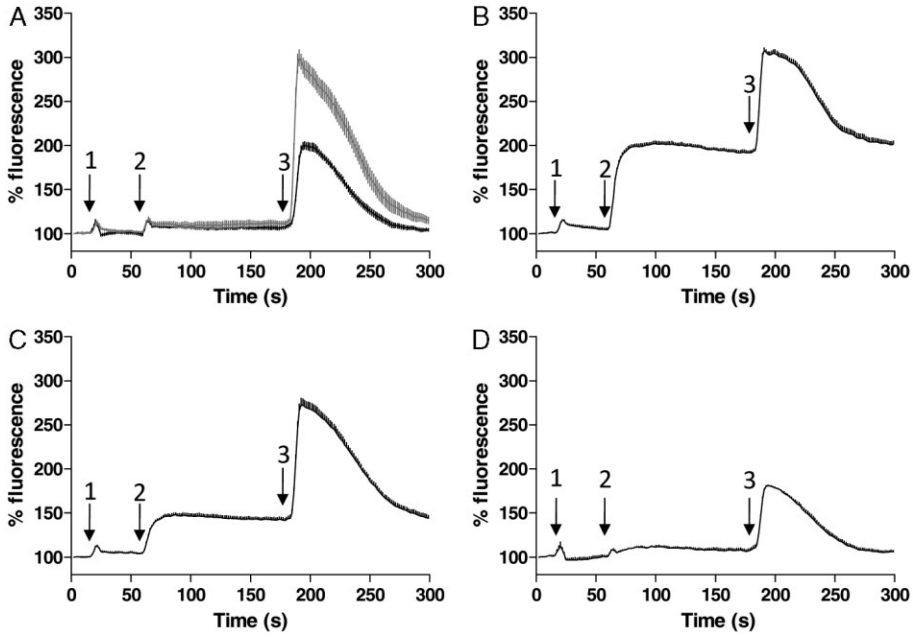

Figure 5

Effect of *h*26RFa on $[Ca^{2+}]_i$ in wild-type or mutant *h*GPR103 transfected CHO cells. Representative curves showing variations of $[Ca^{2+}]_i$ induced by administration of buffer (negative control) at 17 s (arrow 1), *h*26RFa (10^{-6} M) at 60 s (arrow 2) and ATP (10^{-4} M) (positive control) at 180 s (arrow 3) in non-transfected host CHO cells (A, grey line), in tpCHO cells (A, black line), in s*h*GPR103-CHO cells (B), in t*h*GPR103-CHO cells (C) and in tA*h*GPR103-CHO cells (D). Data are mean ± SEM of at least three independent experiments performed in triplicate.

Table 2

Chemical data for Arg^{25}-substituted $26RFa_{(20–26)}$ analogues

		HPLC		MS	
Peptide	**Code**	**t_R (min)[a]**	**Purity (%)**	**Calcd[b]**	**Obsd[c]**
*h*26RFa	LV-2002	27.3	100	2830.45	2831.26
$26RFa_{(20–26)}$	LV-2021	19.3	100	815.41	816.41
$[Lys^{25}]26RFa_{(20–26)}$	LV-2108	18.3	100	787.92	788.38
$[Orn^{25}]26RFa_{(20–26)}$	LV-2109	18.2	100	773.89	774.48
$[Cit^{25}]26RFa_{(20–26)}$	LV-2174	18.6	100	816.92	817.32
$[ADMA^{25}]26RFa_{(20–26)}$	LV-2185	19.1	100	843.98	844.46
$[SDMA^{25}]26RFa_{(20–26)}$	LV-2199	18.7	100	843.98	844.46

[a]Retention time determined by RP-HPLC. [b]Theorical monoisotopic molecular weight. [c]m/z [MH^+] value assessed by MALDI-TOF-MS. Cit, citrulline; Orn, ornithine.

a citrulline moiety led to analogues (LV-2108, LV-2109 and LV-2174, respectively) that were totally devoid of agonistic and antagonistic activity in the calcium mobilization assay (Table 3). Similarly, substitution of the Arg^{25} residue by a symmetrical dimethyl arginine generated the analogue $[SDMA^{25}]26RFa_{(20–26)}$ (LV-2199) that did not exhibit any agonistic or antagonistic activity, whereas introduction of an asymmetrical dimethyl arginine led to $[ADMA^{25}]$ $26RFa_{(20–26)}$ (LV-2185) that reduced by 67.5% *h*26RFa-evoked $[Ca^{2+}]_i$ increase with an IC_{50} of 5.1 ± 1.1 µM (Table 3, Figure 6).

Discussion and conclusion

There is now compelling evidence that the neuropeptide 26RFa (QRFP) and its cognate receptor GPR103 are implicated in the regulation of several physiological functions including energy homeostasis and bone mineralization (see Chartrel *et al.*, 2011; Leprince *et al.*, 2013). To further characterize this peptidergic system, identification of receptor residues that are involved in ligand binding and receptor activation is a fundamental step for understanding the principles of ligand-receptor recognition.

Table 3

Effect of Arg^{25}-substituted 26RFa$_{(20–26)}$ analogues on basal $[Ca^{2+}]_i$ and *h*26RFa-induced $[Ca^{2+}]_i$ increase in *sh*GPR103-CHO cells

Compounds	Amino acid formula of residue 25	Agonist		Antagonist		
		EC_{50} (nM)[a]	pEC_{50}	IC_{50} (nM)[a]	pIC_{50}	Max effect (%)[b]
*h*26RFa, LV-2002	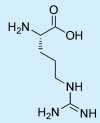	10.4 ± 1.5	8.10 ± 0.04	nd		
26RFa$_{(20–26)}$, LV-2021		739 ± 149***	6.40 ± 0.09	nd		
[Lys^{25}]26RFa$_{(20–26)}$ LV-2108	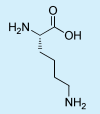	>10^5		>10^5		
[Orn^{25}]26RFa$_{(20–26)}$ LV-2109	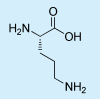	>10^5		>10^5		
[Cit^{25}]26RFa$_{(20–26)}$ LV-2174	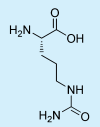	>10^5		>10^5		
[SDMA^{25}]26RFa$_{(20–26)}$ LV-2199	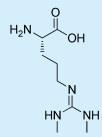	>10^5		>10^5		
[ADMA^{25}]26RFa$_{(20–26)}$ LV-2185	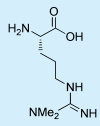	>10^5		5140 ± 1100	5.30 ± 0.11	67.5

[a]Data are the mean ± SEM of at least three distinct experiments performed in triplicate. [b]The maximal effect, at a concentration of $10^{-4.5}$ M, is expressed as a percentage of the mean calcium response inhibition induced by 10^{-6} M *h*26RFa. ***$P < 0.001$ versus control as assessed by Mann and Whitney test. Cit, citrulline; nd, not determined; Orn, ornithine.

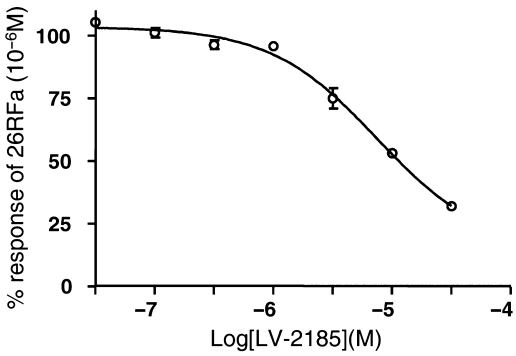

Figure 6

Effect of graded concentration of [ADMA^{25}]26RFa$_{(20–26)}$ (LV-2185) on the *h*26RFa-evoked intracellular calcium increase in *sh*GPR103-CHO cells. Data are mean ± SEM of at least three independent determinations. The values are expressed as percentages of the response induced by 10^{-6} M 26RFa. The pIC_{50} value calculated from the data was 5.30 ± 0.11 for [ADMA^{25}]26RFa$_{(20–26)}$ (LV-2185).

Taking advantage of the high-resolution structure of the human β_2-adrenoceptor that shares 26% sequence identity with *h*GPR103, we have developed a homology model for the *h*26RFa receptor that was subsequently used for ligand docking studies. These comparative models of GPCRs in combination with side-directed mutagenesis are commonly used to provide a molecular template for both ligand binding and functional studies (Chakraborty *et al.*, 2012; Heifetz *et al.*, 2012). In very much the same way as the human β_2-adrenoceptor, our GPR103 model exhibited a relatively narrow and deep binding pocket for accommodating its cognate ligand. Among the solved GPCR structures available, the main structural differences are located in the ECLs. Notably, ECL2, which links the TM4 and TM5 domains, adopts different conformations. In contrast to the buried β-sheet characterized in rhodopsin, the ECL2 of the *h*GPR103 model was strongly exposed to the solvent and contained an extra helical segment (from Ile^{188} to Lys^{196}) named EH that is also present in the β_2-adrenoceptor (Figure 1 and 2A). While the length, sequence and secondary structure of ECL2 vary, a conserved disulfide bridge connecting ECL2 with the top of

TM3 is present in all solved GPCR structures. Numerous studies have shown that this disulfide bond is critical not only for GPCR folding and surface localization, but also for ligand binding (de Graaf *et al.*, 2008). Therefore, sequence alignment of ECL2 in our model was carried out in order to maintain the disulfide bond between Cys^{118} (TM3 domain) and Cys^{201} (ECL2). The *h*GPR103 model exhibited a second non-TM helix in the intracellular extremity between residues Glu^{337} and Val^{347}, named IH. In other GPCRs, it has been shown that IH is involved in receptor signalling. In particular, the IH of rhodopsin, adrenoceptors and angiotensin II receptors is implicated in G-protein coupling and activation (Munch *et al.*, 1991; Sano *et al.*, 1997; Ernst *et al.*, 2000; Lu *et al.*, 2002; Katragadda *et al.*, 2004). IH is also important for phosphorylation of the C-terminal tail of class A GPCRs by GPCR kinases as well as for arrestin recruitment (Gehret *et al.*, 2010; Kirchberg *et al.*, 2011).

We have previously shown that the α-helix of *h*26RFa (Pro^{4}-Arg^{17}) cannot activate *h*GPR103, while the C-terminal region of the peptide is essential for biological activity (Le Marec *et al.*, 2011). Preliminary results showed that the α-helix of *h*26RFa, characterized in methanol (Thuau *et al.*, 2005), extends over two additional residues, in its C-terminal side, up to the Lys^{19} residue in diphosphocholine micelles (A. Marotte, unpubl. data). To get insight as to how the peptide helix stands in *h*GPR103, we have used the (19–26) fragment of *h*26RFa ($26RFa_{(19–26)}$) for docking simulations into the homology model of *h*GPR103. These docking experiments revealed that $26RFa_{(19–26)}$ bound in two different orientations in the ligand-binding pocket within the TM bundle. Both of these binding modes displayed excellent structural complementarities between the ligand and the receptor with numerous intermolecular interactions. According to the docking results, the C-terminal part of $26RFa_{(19–26)}$ sank in depth into the cavity while the Lys^{19} residue remained at the receptor surface. In the first mode, the side chain of the Phe^{26} residue of $26RFa_{(19–26)}$ faced the Gln^{125} moiety of *h*GPR103 while the Arg^{25} residue established an interaction with the Ser^{126} moiety through its Nε atom. In the second mode, the Phe^{26} residue faced a hydrophobic area (Ile^{218}, Leu^{222}, Val^{129} and Val^{130}) and the Arg^{25} residue strongly interacted with the Gln^{125} side chain via its two Nζ atoms. The existence of multiple active conformations has been previously described for other GPCR systems, where agonists, that favour one signalling pathway over another, have been characterized (Galandrin *et al.*, 2007; Rajagopal *et al.*, 2010). We therefore hypothesize that *h*GPR103 exists in different active conformations depending on *h*26RFa fitting, leading to the activation of different signalling pathways. In support of this hypothesis, it has been reported that 26RFa/43RFa stimulated $[Ca^{2+}]_i$ and inhibited cAMP formation via $G_{i/0}$ and/or G_q protein (Fukusumi *et al.*, 2003; Jiang *et al.*, 2003). Moreover, we have recently shown that *h*26RFa displaces ^{125}I-*h*26RFa binding with an IC_{50} of 1.11 nM (Neveu *et al.*, 2012). In the light of the two docking solutions, the data were refitted using an equation for displacement of radioligand by competitors from two binding sites. Interestingly, the two-site curve-fitting model fitted the data significantly better than the one-site model, as determined by an *F*-test at a significance level of $P < 0.05$ ($P = 0.015$), suggesting the existence of a heterogeneous population of binding sites. Taken together, these findings suggest that *h*26RFa may act as a biased agonist of *h*GPR103, that is an agonist that stabilizes distinct receptor conformations that differ in their signalling partner preference, leading to different biological responses as recently shown for the βbeta2-adrenoceptor (Liu *et al.*, 2012), the cholecystokinin CCK-2 receptor (Magnan *et al.*, 2011) and the somatostatin sst-2 receptor (Cescato *et al.*, 2010). However, it should be noted that the difference of affinity between the two *h*26RFa binding sites (IC_{50} –1 = 0.3 ± 0.2 nM; IC_{50} –2 = 7.9 ± 0.3 nM) is relatively low. Thus, the existence of high- and low-affinity binding sites for *h*26RFa deserves further investigation.

As mentioned earlier, the modelling of ECL2 was more complex, because of its length and its low-sequence homology with its counterpart in the human β_2-adrenoceptor. Consistent with the selected $26RFa_{(19–26)}$ position in the *h*GPR103 active site, if the whole *h*26RFa sequence is superimposed on the $26RFa_{(19–26)}$ docked part, the N-terminal amphipathic helix will be situated outside the binding cavity of the receptor, close to ECL2. Taking into account the amphipathy of both the *h*26RFa and ECL2 α-helices, it is possible that interactions occur between these helices at the surface of *h*GPR103 (Figure 7).

In the selected solution, the strongest interaction between $26RFa_{(19–26)}$ and the receptor inside the binding pocket involved the Gln^{125} residue located close to the N-terminal region of the TM3 helix. Interestingly, sequence alignment of human RFamide peptide receptors shows that this Gln residue is fully conserved in all receptors of this superfamily, indicating that all these receptors may present common recognition or activation processes (Figure 8). As the Gln^{125} residue was paired with the Arg^{25} moiety, and as the latter is part of the RFamide motif that is common to all ligands for

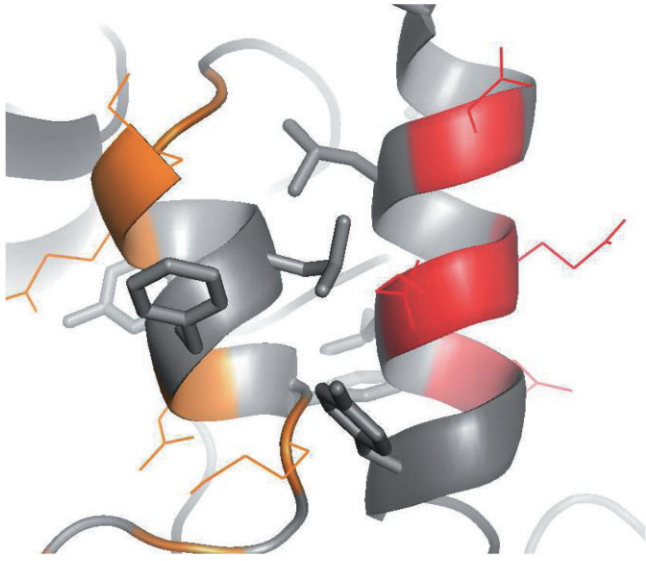

Figure 7

Top view of the proposed position of the amphipathic helix of *h*26RFa on the extracellular surface of *h*GPR103. The EH and the N-terminal helix of *h*26RFa are represented by ribbons. Hydrophobic residues are coloured in grey and charged residues in orange and red for *h*GPR103 and *h*26RFa helices respectively. The figure was drawn with PYMOL, version 1.1eval (DeLano Scientific, 2002).

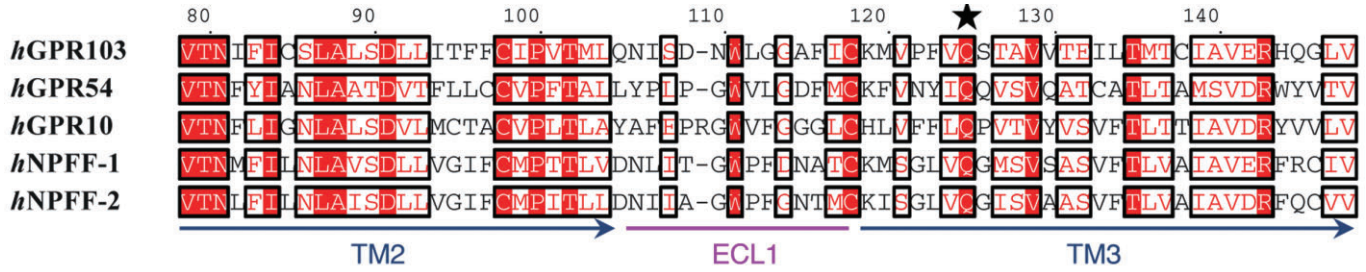

Figure 8

Sequence alignment of the different members of the human RFamide peptide receptor superfamily between residue 79 and residue 148 of *h*GPR103. *h*GPR103, *h*26RFa receptor; *h*GPR54, metastin/kisspeptin receptor; *h*GPR10, prolacting-releasing peptide receptor; *h*NPFF-1, neuropeptide FF/RFRP1 receptor; *h*NPFF-2, RFRP-3 receptor. The conserved Gln^{125} residue is highlighted by a star. Fully conserved amino acids are highlighted with red boxes and highly conserved amino acids with white boxes.

these receptors, we assumed that the Arg/Gln interaction plays a crucial role in receptor binding and/or activation. To test this hypothesis, we constructed the Q125A mutant of *h*GPR103 and evaluated the effect of *h*26RFa on its activation. The mutation and the addition of the C-terminal M2 flag did not affect the expression of the wild-type and mutant *h*GPR103 transcripts, but may modify the trafficking of the recombinant protein as shown by the subcellular distribution of wild-type and mutant tagged *h*GPR103 in transiently transfected CHO cells through confocal microscopy analysis. Of note, the C-terminal M2 flag did not affect the occurrence of *h*GPR103 at the plasma membrane (Chartrel *et al.*, 2011). The recombinant wild-type and Q125A-substituted *h*GPR103 were similarly located at the plasma membrane although, in the absence of a ligand, both receptors were primarily trapped in the intracellular network, most probably in the endoplasmic reticulum. Similar observations have been recently reported for apelin receptor mutants transfected in the same host cells (Iturrioz *et al.*, 2010). However, in the presence of cycloheximide (which by itself had no effect), *h*26RFa provoked an increase in fluorescence at the cellular membrane of wild-type *h*GPR103-transfected cells. These results suggest that activation of *h*GPR103 by *h*26RFa, initially present in small amounts at the cell surface, induces a signalling cascade leading to receptor recruitment from cytosolic stores to the plasma membrane. This agonist-induced regulation of the density of GPCRs at the cell surface has already been reported for many receptors such as the dopamine D_1 receptor, opiate receptors and thrombin receptor (Brismar *et al.*, 1998; Holtbäck *et al.*, 1999; Cahill *et al.*, 2007; Achour *et al.*, 2008). Mutation of the Gln^{125} residue by an alanine in the TM3 domain of *h*GPR103 totally suppressed *h*26RFa-evoked recruitment of the receptor at the plasma membrane, confirming that Gln^{125} is a key amino acid for ligand recognition and/or receptor activation. It has been recently proposed that the positively charged arginine side chain of the C-terminal motif of RFamide peptides interacts with a Glu residue of their cognate receptor located at the extremity of TM6 domain close to EL3 (Findeisen *et al.*, 2011a). As this amino acid is well conserved in RFamide peptide receptors, and as it is involved in NPY-receptor binding (Merten *et al.*, 2007), it has been mutated in all RFamide peptide receptors (Findeisen *et al.*, 2011a,b). Site-directed mutation of Glu^{297} of GPR103 with an alanine partly reduces the 26RFa effect (Findeisen *et al.*, 2011a). The *h*GPR103 model and docking study described herein strongly suggest that the side chain of the Lys^{19} moiety of *h*26RFa rather than the Arg^{25} residue interacts with this glutamic acid located in the ECL3 of the receptor template (Figure 2E). In support of this hypothesis, the Cα of the Lys^{19} residue of $26RFa_{(19–26)}$ was 8 Å apart from that of the Glu^{297} moiety of *h*GPR103, whereas the distance between the Cα of the Arg^{25} residue and the Cα of the Glu^{297} moiety was 14 Å. As the Lys^{19} and Glu^{297} side chains were oriented in opposite directions in the *h*GPR103 model, the amine and carboxylic groups were at a considerable distance from each other. However, the N-terminal part of *h*26RFa, that was missing in our simulations, may introduce a rearrangement of these side chains, leading to a favourable interacting distance between their chemical functions.

In order to determine if the main Arg^{25}/Gln^{125} interaction is implicated in *h*GPR103 activation, we designed five Arg-modified $26RFa_{(20–26)}$ analogues. Replacement of the Arg^{25} residue by a mono-functional and/or a short side chain moiety was deleterious for $26RFa_{(20–26)}$ effect on wild-type *h*GPR103, suggesting that the peptide needs at least two anchoring points for efficient interactions with the receptor. More importantly, from the observation that $[ADMA^{25}]26RFa_{(20–26)}$ (LV-2185) exhibited antagonistic activity, we can assume that the Arg^{25}/Gln^{125} interaction is primarily involved in receptor activation. In addition, these data indicate that chemical modifications of the Arg^{25} moiety of *h*26RFa may yield selective and potent *h*GPR103 antagonists.

In conclusion, the present docking and site-directed mutagenesis studies reveal that the Gln^{125} residue in TM3 domain of *h*GPR103 is involved in the interaction of the receptor with the Arg^{25} residue of the C-terminal motif of *h*26RFa. This crucial Arg^{25}/Gln^{125} interaction between *h*26RFa and its receptor can be exploited for the rational design of selective GPR103 agonists and antagonists.

Acknowledgements

This study was supported by INSERM (U982), the European Regional Development Fund (ERDF – PeReNE) and the Région Haute-Normandie. The authors thank the CRIHAN (Centre

de Ressources Informatiques de Haute-Normandie) for the molecular modelling software. C. N. was the recipient of a fellowship from the Lille-Amiens-Caen-Rouen-Neuroscience Network.

Author contributions

J. L. and J. S-d. O. S conceived and designed the study. Data were acquired by C. N., F. D., B. L., L. Ga., C. C. and L. Gu. Data were analysed and interpreted by C. N., F. D., L. Ga., J. C. and I. S.-M. The paper was drafted by C. N., F. D., J. S.-d. O. S. and J. L. Critical revisions were contributed by R. B., S. R., J. A. B., D. V., H. V. and J. L.

Conflict of interest

The authors disclose no conflict of interest.

References

Achour L, Labbé-Jullié C, Scott MG, Marullo S (2008). An escort for GPCRs: implications for regulation of receptor density at the cell surface. Trends Pharmacol Sci 29: 528–535.

Alexander SPH, Benson HE, Faccenda E, Pawson AJ, Sharman JL, Spedding M *et al.* (2013). The Concise Guide to PHARMACOLOGY 2013/14: G Protein-Coupled Receptors. Br J Pharmacol 170: 1459–1581.

Baribault H, Danao J, Gupte J, Yang L, Sun B, Richards W *et al.* (2006). The G-protein-coupled receptor GPR103 regulates bone formation. Mol Cell Biol 26: 709–717.

Brismar H, Asghar M, Carey RM, Greengard P, Aperia A (1998). Dopamine-induced recruitment of dopamine D1 receptors to the plasma membrane. Proc Natl Acad Sci USA 95: 5573–5578.

Brooks BR, Bruccoleri RE, Olafson BD, States DJ, Swaminathan S, Karplus M (1983). CHARMM: a program for macromolecular energy, minimization, and dynamics calculations. J Comput Chem 4: 187–217.

Bruzzone F, Lectez B, Tollemer H, Leprince J, Dujardin C, Rachidi W *et al.* (2006). Anatomical distribution and biochemical characterization of the novel RFamide peptide 26RFa in the human hypothalamus and spinal cord. J Neurochem 99: 616–627.

Bruzzone F, Lectez B, Alexandre D, Jegou S, Mounien L, Tollemer H *et al.* (2007). Distribution of 26RFa binding sites and GPR103 mRNA in the central nervous system of the rat. J Comp Neurol 503: 573–591.

Cahill CM, Holdridge SV, Morinville A (2007). Trafficking of delta-opioid receptors and other G-protein-coupled receptors: implications for pain and analgesia. Trends Pharmacol Sci 28: 23–31.

Cescato R, Loesch KA, Waser B, Macke HR, Rivier JE, Reubi JC *et al.* (2010). Agonist-biased signaling at the sst2A receptor: the multi-somatostatin analogs KE108 and SOM230 activate and antagonize distinct signaling pathways. Mol Endocrinol 24: 240–249.

Chakraborty R, Pydi SP, Gleim S, Dakshinamurti S, Hwa J, Chelikani P (2012). Site-directed mutations and the polymorphic variant Ala160Thr in the human thromboxane receptor uncover a structural role for transmembrane helix 4. PLoS ONE 7: e29996.

Chartrel N, Dujardin C, Anouar Y, Leprince J, Decker A, Clerens S *et al.* (2003). Identification of 26RFa, a hypothalamic neuropeptide of the RFamide peptide family with orexigenic activity. Proc Natl Acad Sci USA 100: 15247–15252.

Chartrel N, Alonzeau J, Alexandre D, Jeandel L, Alvear-Perez R, Leprince J *et al.* (2011). The RFamide neuropeptide 26RFa and its role in the control of neuroendocrine functions. Front Neuroendocrinol 32: 387–397.

Chomczynski P, Sacchi N (1987). Single-step method of RNA isolation by acid guanidinium thiocyanate-phenol-chloroform extraction. Anal Biochem 162: 156–159.

Eisenberg D, Luthy R, Bowie JU (1997). VERIFY3D: assessment of protein models with three-dimensional profiles. Methods Enzymol 277: 396–404.

Ernst OP, Meyer CK, Marin EP, Henklein P, Fu WY, Sakmar TP *et al.* (2000). Mutation of the fourth cytoplasmic loop of rhodopsin affects binding of transducin and peptides derived from the carboxyl-terminal sequences of transducin alpha and gamma subunits. J Biol Chem 275: 1937–1943.

Eswar N, Eramian D, Webb B, Shen MY, Sali A (2008). Protein structure modeling with MODELLER. Methods Mol Biol 426: 145–159.

Findeisen M, Rathmann D, Beck-Sickinger AG (2011a). RFamide peptides: structure, function, mechanisms and pharmaceutical potential. Pharmaceuticals 4: 1248–1280.

Findeisen M, Rathmann D, Beck-Sickinger AG (2011b). Structure–activity studies of RFamide peptides reveal subtype-selective activation of neuropeptide FF1 and FF2 receptors. Chem Med Chem 6: 1081–1093.

Fukusumi S, Yoshida H, Fujii R, Maruyama M, Komatsu H, Habata Y *et al.* (2003). A new peptidic ligand and its receptor regulating adrenal function in rats. J Biol Chem 278: 46387–46395.

Galandrin S, Oligny-Longpre G, Bouvier M (2007). The evasive nature of drug efficacy: implications for drug discovery. Trends Pharmacol Sci 28: 423–430.

Gehret AU, Jones BW, Tran PN, Cook LB, Greuber EK, Hinkle PM (2010). Role of helix 8 of the thyrotropin-releasing hormone receptor in phosphorylation by G protein-coupled receptor kinase. Mol Pharmacol 77: 288–297.

Gouet P, Robert X, Courcelle E (2003). ESPript/ENDscript: extracting and rendering sequence and 3D information from atomic structures of proteins. Nucleic Acids Res 31: 3320–3323.

de Graaf C, Foata N, Engkvist O, Rognan D (2008). Molecular modeling of the second extracellular loop of G-protein coupled receptors and its implication on structure-based virtual screening. Proteins 71: 599–620.

Gracy J, Chiche L, Sallantin J (1993). Improved alignment of weakly homologous protein sequences using structural information. Protein Eng 6: 821–829.

Heifetz A, Morris GB, Biggin PC, Barker O, Fryatt T, Bentley J *et al.* (2012). Study of human orexin-1 and -2 G-protein-coupled receptors with novel and published antagonists by modeling, molecular dynamics simulations, and site-directed mutagenesis. Biochemistry 51: 3178–3197.

Holtbäck U, Brismar H, DiBona GF, Fu M, Greengard P, Aperia A (1999). Receptor recruitment: a mechanism for interactions between G protein-coupled receptors. Proc Natl Acad Sci USA 96: 7271–7275.

Iturrioz X, Gerbier R, Leroux V, Alvear-Perez R, Maigret B, Llorens-Cortes C (2010). By interacting with the C-terminal Phe of apelin, Phe255 and Trp259 in helix VI of the apelin receptor are critical for internalization. J Biol Chem 285: 32627–32637.

Jain E, Bairoch A, Duvaud S, Phan I, Redaschi N, Suzek BE *et al.* (2009). Infrastructure for the life sciences: design and implementation of the UniProt website. BMC Bioinformatics 10: 136.

Jiang Y, Luo L, Gustafson EL, Yadav D, Laverty M, Murgolo N *et al.* (2003). Identification and characterization of a novel RF-amide peptide ligand for orphan G-protein-coupled receptor SP9155. J Biol Chem 278: 27652–27657.

Jones G, Willett P, Glen RC (1995). Molecular recognition of receptor sites using a genetic algorithm with a description of desolvation. J Mol Biol 245: 43–53.

Jones G, Willett P, Glen RC, Leach AR, Taylor R (1997). Development and validation of a genetic algorithm for flexible docking. J Mol Biol 267: 727–748.

Jorgensen WL, Chandrasekhar J, Madura JD, Impey RW, Klein ML (1983). Refined TIP3P model for water. J Chem Phys 79: 926–935.

Kampe J, Wiedmer P, Pfluger PT, Castaneda TR, Burget L, Mondala H *et al.* (2006). Effect of central administration of QRFP(26) peptide on energy balance and characterization of a second QRFP receptor in rat. Brain Res 1119: 133–149.

Katragadda M, Maciejewski MW, Yeagle PL (2004). Structural studies of the putative helix 8 in the human beta(2) adrenergic receptor: an NMR study. Biochim Biophys Acta 1663: 74–81.

Kirchberg K, Kim TY, Moller M, Skegro D, Dasara Raju G, Granzin J *et al.* (2011). Conformational dynamics of helix 8 in the GPCR rhodopsin controls arrestin activation in the desensitization process. Proc Natl Acad Sci USA 108: 18690–18695.

Labesse G, Mornon J (1998). Incremental threading optimization (TITO) to help alignment and modelling of remote homologues. Bioinformatics 14: 206–211.

Le Marec O, Neveu C, Lefranc B, Dubessy C, Boutin JA, Do-Rego JC *et al.* (2011). Structure–activity relationships of a series of analogues of the RFamide-related peptide 26RFa. J Med Chem 54: 4806–4814.

Lee DK, Nguyen T, Lynch KR, Cheng R, Vanti WB, Arkhitko O *et al.* (2001). Discovery and mapping of ten novel G protein-coupled receptor genes. Gene 275: 83–91.

Leprince J, Neveu C, Lefranc B, Guilhaudis L, Segalas-Milazzo I, Do Rego JC *et al.* (2013) 26RFa. In: Kastin AJ (ed.). Handbook of Biologically Active Peptides. Elsevier: San Diego, CA, pp. 917–923.

Levit A, Barak D, Behrens M, Meyerhof W, Niv MY (2012). Homology model-assisted elucidation of binding sites in GPCRs. Methods Mol Biol 914: 179–205.

Liu JJ, Horst R, Katritch V, Stevens RC, Wuthrich K (2012). Biased signaling pathways in beta2-adrenergic receptor characterized by 19F-NMR. Science 335: 1106–1110.

Lu ZL, Saldanha JW, Hulme EC (2002). Seven-transmembrane receptors: crystals clarify. Trends Pharmacol Sci 23: 140–146.

MacKerell AD Jr, Bashford D, Bellott M, Dunbrack RL Jr, Evanseck JD, Field MJ *et al.* (1988). All-atom empirical potential for molecular modeling and dynamics studies of proteins. J Phys Chem B 102: 3586–3616.

Magnan R, Masri B, Escrieut C, Foucaud M, Cordelier P, Fourmy D (2011). Regulation of membrane cholecystokinin-2 receptor by agonists enables classification of partial agonists as biased agonists. J Biol Chem 286: 6707–6719.

Merten N, Lindner D, Rabe N, Rompler H, Morl K, Schoneberg T *et al.* (2007). Receptor subtype-specific docking of Asp6.59 with C-terminal arginine residues in Y receptor ligands. J Biol Chem 282: 7543–7551.

Mobarec JC, Sanchez R, Filizola M (2009). Modern homology modeling of G-protein coupled receptors: which structural template to use? J Med Chem 52: 5207–5216.

Munch G, Dees C, Hekman M, Palm D (1991). Multisite contacts involved in coupling of the beta-adrenergic receptor with the stimulatory guanine-nucleotide-binding regulatory protein. Structural and functional studies by beta-receptor-site-specific synthetic peptides. Eur J Biochem 198: 357–364.

Neveu C, Lefranc B, Tasseau O, Do-Rego JC, Bourmaud A, Chan P *et al.* (2012). Rational design of a low molecular weight, stable, potent, and long-lasting GPR103 aza-beta3-pseudopeptide agonist. J Med Chem 55: 7516–7524.

Pawson AJ, Sharman JL, Benson HE, Faccenda E, Alexander SP, Buneman OP *et al.* (2014). The IUPHAR/BPS Guide to PHARMACOLOGY: an expert-driven knowledge base of drug targets and their ligands. Nucleic Acids Research 42 (Database Issue): D1098–1106.

Rajagopal S, Rajagopal K, Lefkowitz RJ (2010). Teaching old receptors new tricks: biasing seven-transmembrane receptors. Nat Rev Drug Discov 9: 373–386.

Rodriguez M, Beauverger P, Naime I, Rique H, Ouvry C, Souchaud S *et al.* (2001). Cloning and molecular characterization of the novel human melanin-concentrating hormone receptor MCH2. Mol Pharmacol 60: 632–639.

Sano T, Ohyama K, Yamano Y, Nakagomi Y, Nakazawa S, Kikyo M *et al.* (1997). A domain for G protein coupling in carboxyl-terminal tail of rat angiotensin II receptor type 1A. J Biol Chem 272: 23631–23636.

Simms J, Hall NE, Lam PH, Miller LJ, Christopoulos A, Abagyan R *et al.* (2009). Homology modeling of GPCRs. Methods Mol Biol 552: 97–113.

Takayasu S, Sakurai T, Iwasaki S, Teranishi H, Yamanaka A, Williams SC *et al.* (2006). A neuropeptide ligand of the G protein-coupled receptor GPR103 regulates feeding, behavioral arousal, and blood pressure in mice. Proc Natl Acad Sci USA 103: 7438–7443.

Thuau R, Guilhaudis L, Ségalas-Milazzo I, Chartrel N, Oulyadi H, Boivin S *et al.* (2005). Structural studies on 26RFa, a novel human RFamide-related peptide with orexigenic activity. Peptides 26: 779–789.

Ukena K, Tachibana T, Iwakoshi-Ukena E, Minakata H, Kawaguchi R, Osugi T *et al.* (2010). Identification, localisation and function of a novel avian hypothalamic neuropeptide, 26RFa, and its cognate receptor, G protein-coupled receptor-103. Endocrinology 151: 2255–2264.

Supporting information

Additional Supporting Information may be found in the online version of this article at the publisher's web-site:

http://dx.doi.org/10.1111/bph.12808

Figure S1 Confocal images showing localization of the Flag M2-tagged *h*GPR103 and Q125A*h*GPR103 in stably and

transiently transfected CHO cells in the presence of cycloheximide. Immunocytochemical labelling was performed with a primary antibody against Flag M2 and a secondary antibody labelled with green-fluorescence Alexafluor 488. Nuclei were stained with DAPI (blue). The Flag M2-tagged receptors were detected in s*h*GPR103-CHO cells (A1), in t*h*GPR103-CHO cells (A2) and in tA*h*GPR103-CHO cells (A3). Scale bars = 10 μm.